AN ENHANCED HYBRID SVPWM WITH ANN-BASED VECTOR CONTROL OF INDUCTION MOTOR USING FPGA

[1]RAJAN.V.R
Assistant Professor, V V College of Engineering, Arasoor, Tisaiyanvilai, Tirunelveli, Tamil Nadu 627657, India,
rajan.vrrp@gmail.com
[2]Dr. K. SELVI
Associate Professor, Thiagarajar College of Engineering, Madurai, Tamil Nadu, 625015, India

Abstract: This scheme envisages an indirect field-oriented control that involves estimation of the rotor flux vector with the use of field-oriented control equations (current model) involving a rotor speed measurement. Up-gradation of the weights of artificial neural network used in getting optimal speed control of an induction motor has been done with the use of back-propagation algorithm. The enhanced hybrid space vector pulse width modulation (HSVPWM) technique is a blend of random pulse width modulation (RPWM) and modified space vector pulse width modulation (SVPWM) techniques considered ideal for performance improvement. Amalgamation of the resultant modified SVPWM reference and the random selection of the carrier between two triangular signals, which has, as its objectives, the disbanding of the acoustic switching noise spectrum with basic components that have gone through improvement, is the fundamental doctrine behind the suggested RPWM referred to as enhanced HSVPWM. Apart from providing an improved vector control under a dynamic change in load, the proposed scheme has also other beneficial features that include reduction in oscillations, harmonics, and switching noise in acoustics. Implementation of this scheme, which is in real time, is carried out using Spartan xc6slx45 FPGA board. Very high speed hardware description language has been used in the implementation. Proof of the viability of the proposed scheme has been provided by the results obtained from the various tests conducted.

Keywords: Induction motor (IM), Artificial neural network (ANN), Variable frequency drive (VFD), Hybrid space vector pulse width modulation (HSVPWM), Very high speed hardware description language (VHDL).

1. Introduction

Currently, three-phase induction motors (IMs) are extensively used in industrial drives. Ruggedness, reliability, and economy in applications are the salient features that facilitate the use [1]. Three-phase squirrel-cage IMs are seen as components of the industrial motion control systems. Most applications that use IMs need variations in speed. But IMs face the problem of the limited ability to run only at their rated speed as a direct connection to the main power supply. This brings in the need for variable-speed drives with the capability of making variations in the rotor speed. The popularity and acceptance of variable-frequency drives (VFDs) in variable-speed drives are increasing in the context of widening energy-saving opportunities. Researches have been slogging to discover VFD-based control strategies that can ensure a good performance in IM drives.

The vector control method is among the most popular methods that have emerged from research efforts. This method has the exclusive ability of decoupling a torque and flux control, which provides a linear control over IM in the shape of a separately excited DC motor; this can offer an improved dynamic response [2]. Effective and crafty control schemes for improved performance of IM have become popular propositions for industry. The use of space vector pulse width modulation (SVPWM) has increased in voltage-fed converter AC machine drives, because of higher harmonics quality and enhanced linear range of operation [3]. However, the complex on-line computation required is of a drawback as it restricts its operation up to several kilo-hertz of switching frequency. Extension of switching frequency is possible through the use of field-programmable gate array (FPGA) together with a simplified algorithm that includes look-up tables, which have the ability to reduce the pulse width resolution, except in situations of saturation where their size is large.

A noteworthy improvement seen in recent terms relates to the implementation of the switching speed of a power semiconductor, meant exclusively for an insulated gate bipolar transistor (IGBT). FPGA-based SVPWM is most appropriate for drives with switching frequency below 10 kHz [4]. But the deterministic PWM (SVPWM) switching of inverters produces disagreeable acoustic switching noise and a mechanical vibration in the rotor. The un-deterministic PWM method (RPWM) spreads harmonic power or the basis of demand from modern drives and variations in basic terms total harmonic distortion (THD) as negligible. A large number of RPWM schemes formed have been the subject matter of investigation. They show features that highlight differences in the incorporation of randomness in the carrier signal. Explanation of a specious random triangular carrier modulation method and its harmonic spread effect has been offered [5]. An improved performance has been seen from a discontinuous PWM method with a larger range of modulation which is the requirement for high power application [6]. Neural networks that show substantial potential to facilitate control are feedback signal processing efforts seen in vector-controlled drives known for good performance. Capability for learning parallel computation and tolerance to faults are some other advantages.

Fu and Li [7] have presented the Levenberg–Marquardt algorithm-based neural network, which is a conventional vector control scheme implemented in dSPACE. Pinto et

al [8] have proposed the star flux orientation. The hybrid neural-network-based conventional SVPWM and PCLPF (programmable cascade low pass filter) provide a source of help for the estimation of flux in vector control implementation. Mitronikas and Safacas [9] have achieved completion of an improvement in sensor-less vector control method for an IM. In zhang and Li [10], a stochastic algorithm (stochastic arithmetic theory)-based FPGA controller has been proposed for an IM drive using integrated feed forward neural network algorithms. But implementation was not done using the vector technique.

Lai and Chang [11] have proposed the vector control using the random switching technique, which does not involve an artificial neural network (ANN). Hu et al [12] succeeded in the implementation of a three-level conventional SVPWM-based IM control with FPGA. Ben-Brahim and Kurosawa [13] have used simulation of a neural network that has, as its bases, a back-propagation algorithm which is required for the identification of the mechanical speed of an IM. But no solution was found to the problem of computing control features that have relation with the current loop. Kim et al [14] implemented a new hybrid random PWM (RPWM) scheme for open loop that disperses the acoustic switching noise spectra of an IM drive. In [15], the authors have elaborately discussed acoustic noise reduction in sinusoidal PWM drives with the use of a randomly modulated carrier.

This article has, as its subject matter, used indirect field-oriented control (IFOC) in the estimation of rotor flux based on field-oriented equations (current model) that need rotor speed measurement. Known for its uniqueness, this process ensures accuracy in flux calculation in the entire gamut of special ranges. Hybrid space vector pulse width modulation (HSVPWM) is used in the shape of the pulse modulation technique, which disperses acoustic switching noise spectrum with enhanced fundamental components through a combination of RPWM and modified SVPWM techniques. A closed-loop estimator is also considered. This estimator assists estimation of rotor speed, using a proximity sensor, with further processing done by ANN whose use is seen only on the outer loop for obtaining improved speed control with accuracy. Torque maintenance is also carried out in the same manner. The use of the PI controller is seen in the current control loop (ie., inner loop) together with the back propagation algorithm-based ANN. Xilinx software in very high speed hardware description language (VHDL) language is used in its implementation with execution by FPGA, which helps simplification to a high degree with an expeditious implementation of a program meant for control as also a feedback processing of an enlarged performance AC drives. The work involving a combination of vector-controlled IM that uses enhanced HSVPWM and ANN alone on speed loop with FPGA is seen as a novel process with features that ensure performance of a higher order. A prototype has been of immense use in the appraisal of the performance of a complex vector-controlled device.

2. System Description

The standard vector control has a nested loop structure. It has an inner current loop known for its speed together with a slower outer speed and a rotor flux loop. The former has a role of great importance in obtaining AC drive of high quality for an IM. The outer speed and rotor flux loop have the role of generating of *d*- and *q*-axis current references to the inner loop controller (which has the function of the ultimate control through a voltage signal to the PWM inverter).

The two-phase currents get ideally aligned with some transformation module (Clarke and Park). The i_α and i_β make up the projection arising from the Clark block. These components enable the input for the Park transformation that provides the current in the d, q rotating reference frame, which fits into the rotor flux vector. The appropriate positioning of the rotor flux angular $\theta^{\lambda r}$ is imperative for computing the two components i_{ds} and i_{qs}, which becomes the subjects of comparison with the references i_{dref} (flux reference) and i_{qref} (the torque reference). i_{qref} is the output of the speed regulator. i_{dref} is the appropriate rotor flux command for every speed reference within the area of the normal value. V_{dref} and V_{qref} are the current regulator outputs come out from the flux reference and torque reference, respectively, which become the inverse Park transformation, whereas $V_{\alpha ref}$ and $V_{\beta ref}$,the components of the stator vector voltage in the α and β orthogonal reference frame, respectively, constitute the output. These form the inputs for the space vector PWM, drive, and inverter. Resistance from the rotor and rotor inductance as parameters are the requirements for the main block of vector control [16-18]. Besides, with highest accuracy, it has a perceptible effect on the performance of the control. A rectifier and three-phase two-level IGBT PWM inverter that generate variable voltage and variable frequency power for the machine form the components of the power circuit. Fig.1. shows the implementation block diagram displaying the FOC drive system.

2.1 The Current Control Model:

A good knowledge of the rotor flux space vector magnitude and position is required for getting control over IM vector, which forms the basis of work for the current model. The following two equations form the basis of work for the current model [19, 20].

$$i_{ds} = T_r \frac{di_{mR}}{dt} + i_{mR} \quad (1)$$

$$f_s = \frac{1}{\omega_b}\frac{d\theta_{\lambda r}}{dt} = n + \frac{i_{qs}}{T_r}\left(\frac{1}{i_{mR}}\right)\left(\frac{1}{\omega_b}\right) \quad (2)$$

where $\theta_{\lambda r}$ is the rotor flux position; i_{mR}, the magnetizing current; and $T_r = \frac{L_r}{R_r}$, the rotor time constant. A good knowledge of this constant considering its close association with the rotor flux speed integrated for getting the rotor flux position forms the basis of the proper functioning of the overall FOC.

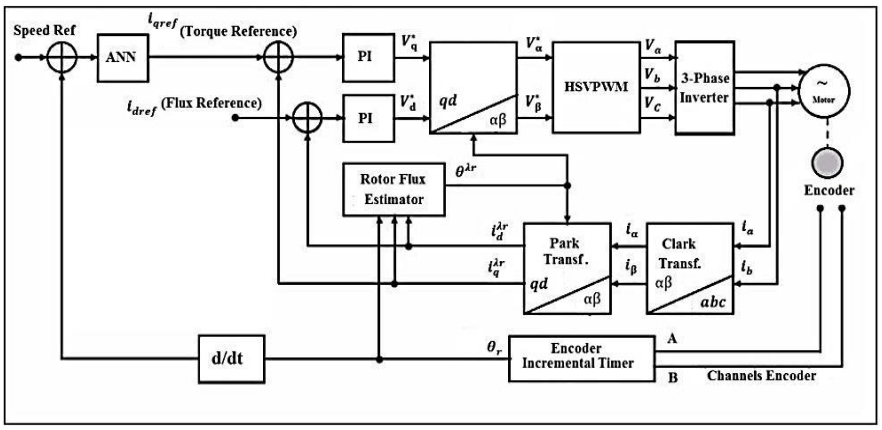

Fig. 1. Implementation block diagram of vector control (IFOC).

Assuming $i_{qS_{k+1}} \sim i_{qS_k}$. Eq. (1) and Eq. (2) can be expressed as follows:

$$i_{mRk+1} = i_{mRk} + \frac{T}{T_r}\left(i_{ds_k} - i_{mR_k}\right) \quad (3)$$

$$f_{s_{k+1}} = n_{k+1} + \left(\frac{1}{T_r}\right)\left(\frac{1}{\omega_b}\right)\left(\frac{i_{qs_k}}{i_{mR_{k+1}}}\right) \quad (4)$$

$$\theta_{\lambda rk+1} = \theta_{\lambda rk} + \omega_b . f_{s_{k+1}} . T \quad (5)$$

The steady-state condition suggests the responsibility of the i_d current component in the generation of the rotor flux. A low-pass filter relationship is seen between the i_d current and the rotor flux, which facilitates transient changes. The magnetizing current, i_{mR} , whose function is the production of rotor flux, is the component of i_d. i_d equals i_{mR} under a steady-state condition. A good understanding of the rotor electrical time constant is the requirement of the equation. The flux producing component of i_d is linked during transient changes through use of the magnetizing current equation.

Computation of the slip frequency seen in Eq. (3) is done with the help of the computed i_{mR} . Work of the slip frequency function is seen with the rotor electrical time constant remaining i_q, i_{mR}, and current rotor velocity. The focus of flux estimator equation, which is used in Eq. (4), is on the expression of the new flux angle on the basis of the slip frequency, which has relation to the equation Eq. (4). The computation of flux angle using earlier specification of IM flux and torque is carried out in a situation that implies the relationship between the slip frequency and stator currents through Eq. (3) and Eq. (4), with an appropriate orientation of the stator currents to the rotor for a specific flux. Maintenance of this orientation facilitates independent control of the flux and torque. Control over motor torque is possible through the i_d current component. The PI controller dominates the current component [19, 20]. The PI algorithm has been written in VHDL as a current control module.

2.2 Neural Controller Design

Approximation of nonlinear functions is done through a group of computing nodes [21], each of which constitutes a neuron. The attachment of each node comprises a multiplication of input signals by constant weights and aggregation of the results and mapping the sum to a function involving non-linear activation. Implementation of ANN on a FPGA controller is the feature of this application.

Fig. 2 is the general block diagram that illustrates recursive ANN training. A series of test inputs presented explain the (possibly unknown) desired function and the ANN. It is possible or desirable to make computation of the prediction error $\varepsilon(k) = y(k) - \hat{y}(k)$ at each time step k. The training algorithm is meant for the use of $\varepsilon(k)$ for adjustment of the weights of the ANN to be of assistance in the reduction of the quadratic $Q(k) = \varepsilon^T(k).\varepsilon(k)$ over time to the minimum. The error back propagation algorithm is extensively used in ANN application enabling achievement of this minimization. The algorithm is the recursive approximation to the algorithm, giving rise to the descent of the steepest magnitude. Calculation of an equivalent error is done for each node in the ANN. The equivalent error δ_m of node m in the output layer is seen in Eq. (6) [22].

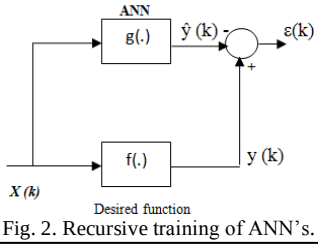

Fig. 2. Recursive training of ANN's.

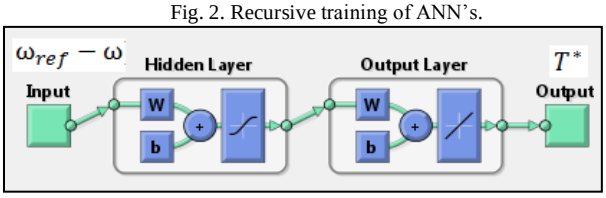

Fig. 3. Structure of ANN.

$$\delta_m(k) = \varepsilon_m(k) = y_m(k) - \hat{y}_m(k) \quad (6)$$

The equivalent error δ_j of node j in the hidden layer is seen Eq. (7).

$$\delta_j(k) = \frac{d_a(z_{j(k)})}{dz_j(k)} \sum_m \delta_m(k)\omega m_j(k) = h_j(k)[1 - h_j(k)] \sum_m \delta_m(k)\omega m_j(k) \quad (7)$$

Weights linking the hidden and output layers are

adjusted as seen in Eq. (8)

$$\Delta_{mj}(k) = \gamma_m \Delta_{mj}(k-1) + \gamma_g \delta_m(k) h_j(k)$$
$$\omega_{mj}(k+1) = \omega_{mj}(k) + \Delta_{mj}(k) \quad (8)$$

where, and γ_g are the momentum and the gain parameters, respectively. Weights connecting the inputs to the hidden layer get adjusted on the basis of Eq. (9).

$$\Delta_{ij}(k) = \gamma_m \Delta_{ij}(k-1) + \gamma_g \delta_j(k) x_j(k)$$
$$\omega_{ji}(k+1) = \omega_{ji}(k) + \Delta_{ji}(k) \quad (9)$$

The calculation of the output layer error using Eq. (6) is the first step in the process. The next is the back propagation using the ANN with Eq. (7) for computation of the equivalent error of the hidden nodes. Adjustment of the ANN weights is done using Eq. (8) and Eq. (9). The structure of the neural controller used in this implementation is shown in Fig. 3.

Speed error is the input to the NN controller. Logarithmic sigmoid has the responsibility of doing the activation function for the input and hidden layer neurons. It is linear for the output neuron. A single-variable nonlinear function signified by IOF (input output function) enables representation of the relationship between the start-up and the load disturbance. It is expressed by:

$$T^* = \mathrm{IOF}(\omega_{ref} - \omega) \quad (10)$$

Achievement and estimation of this are possible with the NN, as shown in Fig. 3. The use of the back-propagation algorithm helps obtain neuron weights and biases of the network parameters. This algorithm does an iterative adaptation of weights of the network till a stage is needed when the error between target vectors and the output of the ANN becomes very small in comparison with an error goal. This is the method used for storage of sigmoidal function value for different speed errors in the lookup table in FPGA. Retrieval of these values is done with respect to the speed error manipulated with weight, and given subsequently in the form of neural network as the outcome of a numerical controller that provides output as T^*(Torque reference) in the indirect field-oriented IM drive control structure, as shown in Fig. 1.

2.3 Conventional Space Vector Pulse Width Modulation:

The implementation of conventional SVPWM is as follows [21],

$$V_S = \left(\frac{T_0}{T_S} \times V_0\right) + \left(\frac{T_1}{T_S} \times V_1\right) + \left(\frac{T_2}{T_S} \times V_2\right) + \left(\frac{T_3}{T_S} \times V_3\right) + \left(\frac{T_4}{T_S} \times V_4\right) + \left(\frac{T_5}{T_S} \times V_5\right) + \left(\frac{T_6}{T_S} \times V_6\right) + \left(\frac{T_7}{T_S} \times V_7\right) \quad (11)$$

$$T_S = T_0 + T_1 + T_2 + T_3 + T_4 + T_5 + T_6 + T_7 \quad (12)$$

$$V_S = \left(\frac{T_A}{T_S} \times V_1\right) + \left(\frac{T_B}{T_S} \times V_2\right) + \left(\frac{T_{0/7}}{T_S} \times V_{0/7}\right) \quad (13)$$

$$T_S = T_A + T_B + T_{0/7} \quad (14)$$

The time intervals $T_A, T_b, T_{0/7}$ require working out for obtaining the guarantee of the identical feature of the average volt second produced by the vector $V_1, V_2, V_{0/7}$ along the X and Y axes and the average volt second produced by the desired reference space vector V_S.

The modulation index, $$m = \frac{|Vs|}{V_{DC}} \quad (15)$$

$$(V_{DC} \times T_A) + (V_{DC} \times \cos\tfrac{\pi}{3} \times T_B) = |Vs| \times \cos\psi \times T_S \quad (16)$$

$$(V_{DC} \times \sin\tfrac{\pi}{3} T_B) = |Vs| \times \sin\psi \times T_S \quad (17)$$

Solving T_A and T_B we get

$$\frac{T_A}{T_s} = \frac{2}{\sqrt{3}} m \times \sin(\tfrac{\pi}{3} - \psi) \quad (18)$$

$$\frac{T_A}{T_s} = \frac{2}{\sqrt{3}} m \times \sin\psi \quad (19)$$

These symmetries explain the lower THD in SVPWM.

$$m_{max} = \frac{V_{DC}}{V_{DC}} \cos\frac{\pi}{6} = \frac{\sqrt{3}}{2} \quad (20)$$

Maximum line to line voltage $= \frac{2}{\sqrt{3}} \times m_{max} \times V_{DC}$

$$= \frac{2}{\sqrt{3}} \times \frac{\sqrt{3}}{2} \times V_{DC} \quad (21)$$

Getting line-to-line voltage of magnitude equal to V_{DC} is possible using the SVPWM algorithm in the linear operating range. This is shown in Eq. (21). The SVPWM algorithm alone has this advantage, in comparison with sine PWM. The higher line-to-line voltage amplitude produces higher torque from the motor. It is a better dynamic response from the motor. The conventional symmetrical SVPWM waveforms in six space sectors are shown in Fig. 4.

2.4 Modified Space Vector Modulation:

Complex computation in conventional SVPWM is avoided using the modified SVPWM. Its operation gets limited to several kilo-hertz of switching frequency. This modified SVPWM scheme, which has application in two-level inverters, compares each reference phase voltage V_s with the triangular carrier, in sharp contrast to the generation of the individual phase voltages that are mutually independent [24, 25]. Addition of a common mode voltage $V_{offset1}$ is made to the reference phase voltages for avoiding the advantages of the maximum possible peak amplitude of the fundamental phase voltage in linear modulation. The amplitude of $V_{offset1}$ here is expressed as:

$$V_{offset1} = -\left(\frac{V_{max} + V_{min}}{2}\right) \quad (22)$$

$$V_{XN}^* = V_{XN} + V_{offset1}, \text{ for } X = A, B, C \quad (23)$$

V_{min} is minimum of $V_{AN} V_{BN} V_{CN}$; V_{max} is maximum of $V_{AN} V_{BN} V_{CN}$

In Eq. (22), V_{max} refers to the quadrature of the three sampled reference phase voltages at a sampling interval whereas V_{min} is the minimum. The addition of the common mode voltage, $V_{offset1}$, leads to the creation of active inverter switching vectors in a sampling interval of the modified SVPWM technique.

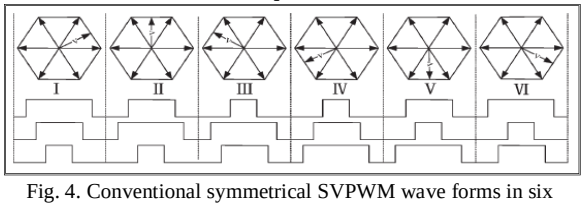

Fig. 4. Conventional symmetrical SVPWM wave forms in six space sectors.

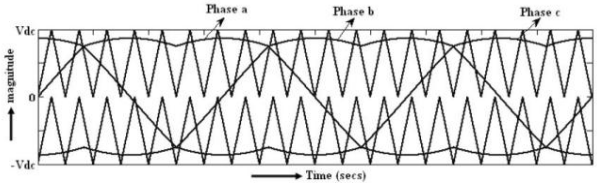

Fig. 5. Modified reference with triangular carriers for inverters.

A solution for determination of the time instants indicating the crossing of three reference phases over the triangular carriers is provided by the modified reference SVPWM techniques. These time analyses are sorted to find the offset voltage, which is to be added to the reference phase voltages for SVPWM generation for inverters for the entire range of linear modulation. The idea is to center the middle inverter in switching vectors during a sampling interval. This is seen in the two-level modified SVPWM scheme regarded as traditional. Fig. 5 shows the modified reference with triangular carriers for inverters.

2.5 Random Carrier Pulse Width Modulation:

The generation of spiteful acoustic switching noise and a mechanical vibration by the motor are offshoots of the deterministic PWM (modified SVPWM) switching of the inverters. Increase in the switching frequency up to 20 kHz is the ideal way for ensuring reduction in the audible switching noise dispersed from the IM. The noise problem finds the solution from the use of this method. As against this, it causes increase in the switching losses of the inverter [26]. This above problem can be solved with RPWM method. A random carrier is obtained through random composition of two triangular carriers, with each having frequency of the same magnitude, but of an opposite phase.

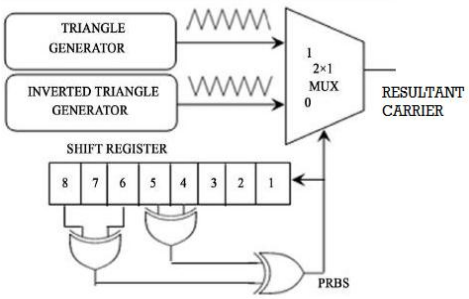

Fig. 6. The carrier generation and selection of carrier.

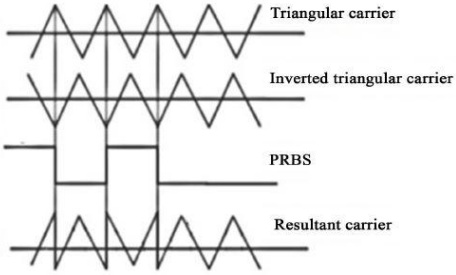

Fig. 7. Random carrier wave generation.

Table 1. Truth Table of the Random Carrier Selection

PRBS status	Max output
0	Triangle
1	Inverted Triangle

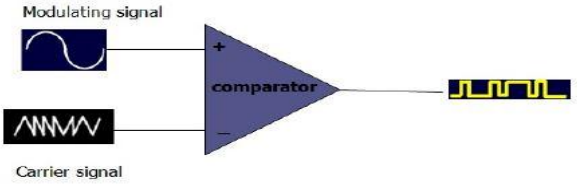

Fig. 8. RPWM Generation.

"Low" or "high" states of the pseudo random binary sequence (PRBS) provide the basis for deciding the random selection of the two cases. Changes in the output of the shift register are common occurrence in every switching cycle. Table 1 is the truth table of the PRBS. Fig 6 shows the carrier generation and selection of a winning carrier. Fig 7 shows the random carrier wave generation. A comparison of the sinusoidal reference with the winning carrier (resultant carrier) helps generation of the random pulse. This is shown in Fig 8. The parameter that does evaluation of harmonic spread effect of the RPWM scheme is HSF (harmonic spread factor) [27].

$$HSF = \sqrt{\frac{1}{N-1}\sum_{j>1}^{N}(H_j - H_O)^2} \qquad (24)$$

$$H_O = \sum_{j>1}^{N} {(H_j)}\Big/{(N-1)}$$

where,'H_j' is j^{th} harmonics amplitude, 'H_0' is average value of all 'N' harmonics. The HSF provides quantitative parameters for the harmonic spectrum spread effect of RPWM scheme with the requirement being the small HSF would be zero for ideally flat spectra of white noise.

2.6 Proposed Enhanced Hybrid SVPWM Scheme:

A resourceful PWM scheme, which is an amalgam of the features of modified SVPWM and RPWM, is useful for any modern AC drive system. The concept of the SVPWM proposes six references (analog equivalent) for most of the THD and the enriched basis without any provision of guidance for carrier selection but with the suggestion of the usage of a conventional triangular carrier. The addition of a randomness feature to the RPWM is seen in the carrier wave, through with restrictions within the carrier cycle. This results in the amalgamation of the random carrier with the modified SVPWM pattern reference. The enhanced HSVPWM proposed by the author involves the computation of its timing of carrier randomness to its existing complexity together with a demand for meticulous care in its implementation.

An enhanced HSVPWM is implemented using the architecture shown in Fig. 10. The architecture has three functional blocks, namely, modified SVPWM reference generator block, carrier generation and selection block, and pulse generation block. The modified SVPWM reference generator block has the function of generating three-phase references. Normal triangular carrier (+fc) with 10 kHz and inverted triangular carrier of same frequency (−fc) are given as inputs to the 2:1 multiplexer in the carrier generation and selection. The output of the linear feedback shift register (LFSR)-based 8-bit random

bit generator is the basis of the triangle referred to as the winning triangle. Solution of the +fc triangle is provided in the event of the output of the carrier generation block is "1" or else, the winning triangle is an –fc triangle. The pulse generation block does a comparison of the modified SVPWM references with the randomized carrier, generating the pulses for the six switches of VSI in the process. The proposed HSVPWM has better performance than the conventional SVPWM and RPWM in terms of fundamental voltage and THD, but in addition, provides HSF of a smaller magnitude, resulting in a reduced acoustic noise. Proof of the noise reduction using HSVPWM is provided by a simulation carried out with the DC bus voltage 600V, switching frequency being 10 kHz, and tested with the 415 V, 1.5 hp, and a three-phase squirrel-cage IM. The simulation results of the harmonic spectra for pattern 1 of the HSVPWM with the speed of 1200 rpm and related to noise spectra are shown in Figs. 9(a) and (b).

Clustered harmonics are a feature with any deterministic PWM with carrier frequency, fc (say 10 kHz) at its multiples (2fc, 4fc, 6fc etc.). This is shown in Fig. 9 (a). The acoustic noise emanated by the motor shows aversion of a high order under this condition, as a result of the majority harmonics coming within the audible range (20 Hz-20 kHz). These clustered harmonic spectra produce acoustic noise, electromagnetic interference (EMI), and mechanical vibration causing physical damage to the rotor. Increase in the PWM switching frequency to 18 Hz is considered as the first step in reducing the audible switching noise that is emitted from the IM, which has the ability to provide a solution to the noise problem but with increase in the switching loss of the inverter.

In general, the 1-10 kHz range is the region in which the worst harmonic spectrum irritation is produced for humans. Unfortunately, coinciding with the switching frequency of the VSI is often likely for this range. This leads to the requirement of a reduction in the acoustic noise radiated from the IM with a frequency lower than 10 kHz. Implementation of the proposal of a new host of technique referred to as HSVPWM can offer a solution to this problem. RPWM being one of the compounds of HSVPWM contributes to precision of harmonics with the same range of switching frequency where occurrence is seen with the use of deterministic PWM methods. RPWM technique has the reputation of operation at variable switching frequency.

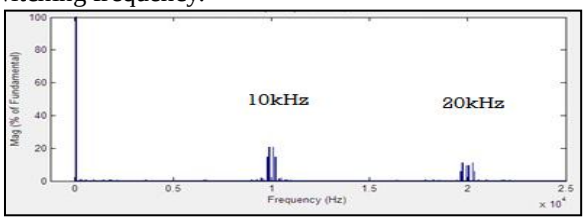

(a)

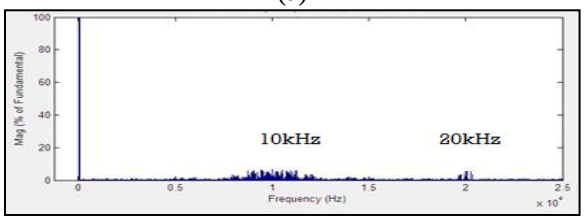

(b)

Fig. 9. Output voltage harmonic spectrum
(a) SVPWM, (b) HSVPWM.

Problems mentioned earlier are mitigated through a random selection of carrier triangle wave. This is illustrated in Fig. 9 (b) as the output of HSVPWM. Attempts at changing the reference wave were made earlier toward the fundamental enhancement and reduction in THD. Reformation of a harmonic spectrum similar to spreading the harmonic power requires carrier modification/randomization. RPWM is the solution to the above referred problems, with the selection of switching frequency within the audible range with an intelligent randomness to ensure the total absence of any forbidden audio noise.

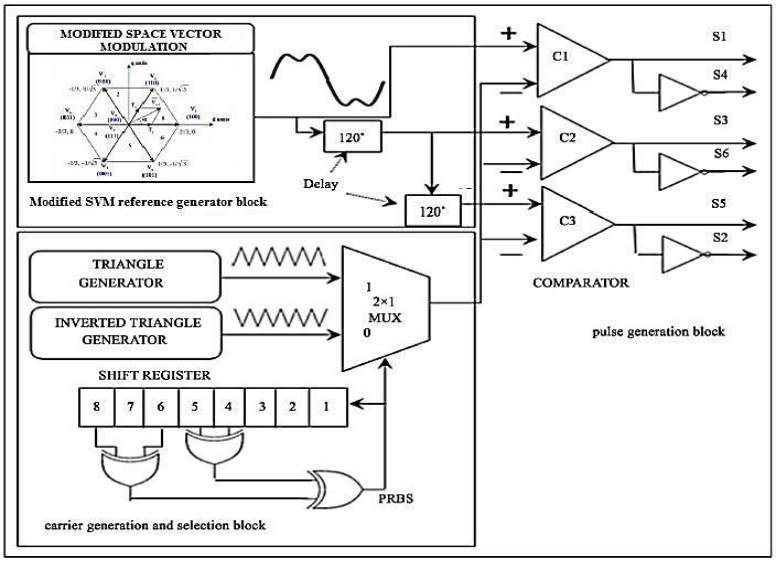

Fig. 10. Proposed enhanced HSVPWM method.

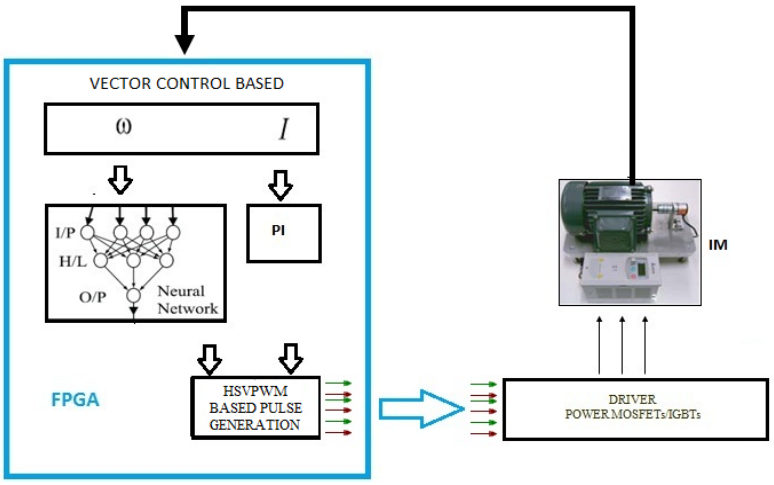

Fig. 11. Top-level logical and hardware block diagram.

3. Hardware Implementation

Implementation of this field-oriented vector control scheme is carried out with Xilinx Spartan-xc6slx45–based FPGA platform. Fig. 11 shows the implemented hardware scheme.

Table 2. Resources and Usages of IP Core

Target Device xc6slx45	Resources on chip	Used resources	%of usage
Slice Registers	54,576	3,467	6%
Slice LUTs	27,288	4,148	15%
Memory	6,408	69	1%
Flip Flops	5,137	3,027	58%

Table 3. Specifications Related to PWM Inverter

DC supply to inverter	600V DC
Switching frequency	10 kHz
Dead time	4 µs
PWM output mode	Symmetrical PWM

Constructs of the top-level design for the two-level enhanced HSVPWM IP involves the use of these functional blocks as the basis, followed by completion, optimization and synthesis with Xilinx software and integration into the FPGA. In this design, the authors' choice is Spartan FPGA xc6slx45 from Xilinx, Inc. Successful compilation of the programming file in (*.bit) format follows the allocation of the pins that use the assignment editor. Direct downloading of this format to FPGA through JTAG is possible using a Xilinx programmer. An FPGA unit can deal with such complex logic operations of PWM signals. But the FPGA uses its effective logical capability for handling these data, generating the HSVPWM signals in the process. This method can be realized on one-chip FPGA. Incorporation of an embedded processor to FPGA ensures better reliability. Table 2 provides a summary of the hardware resources that is especially to the IP core and their uses. The designed IC can operate at 20 MHz, indicating the feasibility of computation for the two-level inverter HSVPWM as short as 50 ns with the addition of the feasibility of switching frequency and the adjustment of dead time. Table 3 shows the specification related to the PWM inverter.

4. Experimental Results

4.1 No-Load Response:

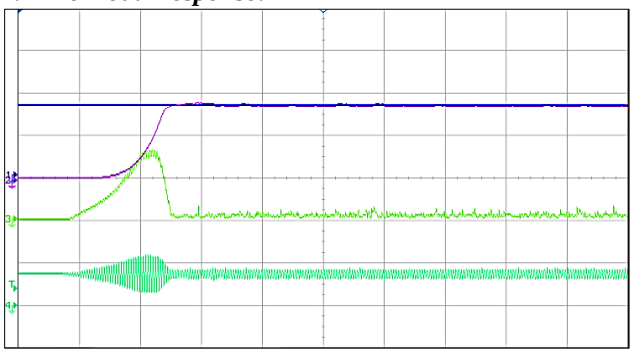

Fig. 12. No-load response at 1200 rpm (Y axis: speed: 1 v/div = 700 rpm; stator current: 2 v/div = 1A); X axis: 200 ms/div).

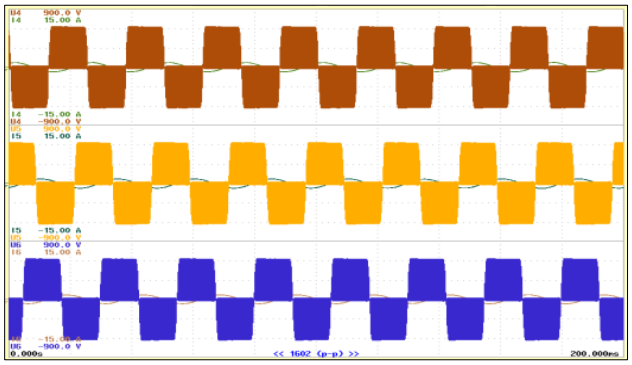

Fig. 13. Stator voltage and stator current wave forms (V_a,V_b,V_c and I_a,I_b,I_c) at the no-load.

The first step is the starting up of the motor without any load but with a reference speed of 1200 rpm set for the purpose. The speed of the motor touches 1200 rpm in 0.45 s with zero peak overshoot and settles at 0.55s with 0.2% error. The torque is also reached steady state at

Table 4. The values of Odd and even harmonics for no-load and dynamic responses

	No load response									Dynamic response (load at 1.8A									
	Frequency – 40.097 Hz									*Frequency – 44.106 Hz*									
	Odd Harmonics					Even Harmonics				Odd Harmonics					Even Harmonics				
Order	V (V)	HDF (%)	I (A)	HDF (%)	Order	V (V)	HDF (%)	I (A)	HDF (%)	Order	V (V)	HDF (%)	I (A)	HDF (%)	Order	V (V)	HDF (%)	I (A)	HDF (%)
1	262.4	99.83	0.8837	99.98	2	1.06	0.403	0.0173	1.957	1	266.9	99.95	1.8026	99.92	2	3.29	1.232	0.0320	1.776
3	1.14	0.432	0.0066	0.742	4	0.75	0.287	0.0030	0.340	3	2.24	0.838	0.0158	0.877	4	1.35	0.505	0.0121	0.673
5	0.95	0.360	0.0024	0.273	6	0.78	0.296	0.0032	0.363	5	0.99	0.372	0.0533	2.956	6	1.22	0.458	0.0042	0.234
7	0.67	0.256	0.0012	0.137	8	0.67	0.256	0.0019	0.210	7	1.33	0.499	0.0276	1.528	8	1.15	0.430	0.0059	0.326
9	0.53	0.200	0.0014	0.159	10	0.21	0.079	0.0007	0.078	9	2.34	0.877	0.0040	0.224	10	0.87	0.325	0.0019	0.104
11	0.12	0.045	0.0004	0.041	12	0.12	0.045	0.0007	0.077	11	2.67	1.002	0.0032	0.179	12	1.82	0.681	0.0024	0.132
13	0.44	0.168	0.0005	0.053	14	0.30	0.115	0.0010	0.111	13	0.54	0.202	0.0014	0.075	14	1.83	0.685	0.0004	0.022
15	0.67	0.257	0.0005	0.053	16	0.42	0.159	0.0011	0.127	15	1.50	0.563	0.0005	0.026	16	0.73	0.272	0.0006	0.036
17	2.18	0.828	0.0004	0.045	18	0.48	0.182	0.0004	0.046	17	1.53	0.574	0.0014	0.077	18	1.67	0.626	0.0007	0.041
19	7.60	2.891	0.0008	0.096	20	2.31	0.880	0.0003	0.033	19	2.16	0.808	0.0007	0.038	20	1.69	0.632	0.0009	0.049
21	1.28	0.487	0.0012	0.134	22	0.63	0.240	0.0002	0.022	21	1.10	0.411	0.0009	0.051	22	0.34	0.127	0.0007	0.041
23	6.36	2.421	0.0004	0.048	24	0.68	0.258	0.0001	0.013	23	1.08	0.405	0.0007	0.041	24	0.79	0.297	0.0007	0.039
25	6.73	2.561	0.0003	0.030	26	0.61	0.231	0.0001	0.015	25	0.79	0.296	0.0005	0.030	26	1.13	0.422	0.0012	0.065
27	0.64	0.243	0.0006	0.069	28	0.76	0.288	0.0003	0.030	27	0.53	0.197	0.0005	0.029	28	0.12	0.043	0.0009	0.050
29	3.58	1.363	0.0003	0.039	30	1.01	0.382	0.0003	0.031	29	0.15	0.055	0.0004	0.021	30	0.42	0.158	0.0010	0.054
31	0.46	0.175	0.0003	0.032	32	0.36	0.136	0.0001	0.010	31	0.44	0.166	0.0006	0.034	32	0.17	0.065	0.0004	0.019
33	0.35	0.133	0.0001	0.009	34	0.27	0.101	0.0001	0.007	33	0.35	0.131	0.0003	0.018	34	0.18	0.066	0.0004	0.023
35	0.37	0.141	0.0001	0.011	36	0.24	0.093	0.0001	0.012	35	0.11	0.043	0.0002	0.010	36	0.15	0.055	0.0003	0.019
37	0.82	0.311	0.0002	0.018	38	0.92	0.348	0.0000	0.004	37	0.23	0.087	0.0004	0.021	38	0.29	0.107	0.0004	0.025
39	1.02	0.388	0.0002	0.024	40	2.78	1.057	0.0002	0.027	39	0.20	0.074	0.0003	0.019	40	0.11	0.042	0.0003	0.017

0.55 s with slight ripples. The inrush current extends up to 0.5s which is very lesser. Calculation of HSF is done using odd and even harmonic values, very much smaller compared to those reported in other [26][29]. There is a substantial reduction in the acoustic noise. Considering the lower value of the harmonics spread factors for voltage and current (HSF_v = 1.6 and HSF_i = 1.5). It is suitable for modern AC drives for noise-free working. This is one of the objectives of this work. Fig. 12 shows the reference speed, actual speed, torque, and stator current of neural-based vector controlled IM. Fig. 13 shows the voltage and current waveforms of each phase (V_a,V_b,V_c and I_a,I_b,I_c). The THD values of stator voltage and current at no load are 5.875 % and 2.213 %.

4.2 Dynamic Response:

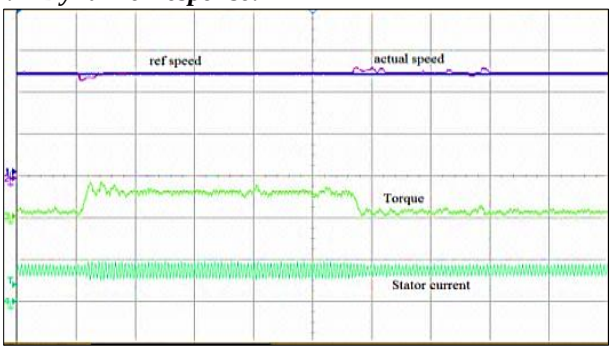

Fig. 14. Speed response of 1200rpm at the load of 1.8 A (Y-axis: speed: 500 mv/div = 500 rpm; stator current: 2 v/div = 2 A); X-axis: 200 ms/div).

Figs. 14–15 show the obtained results of experiment conducted with the starting of the IM with a reference speed of 1200 rpm and with a manual application of a load of 1.8 A. Reduction in this speed of the IM to 1150 rpm is seen with the system getting vector-controlled errors corrected speedily due to the ability of ANN and PI controller. So the speed response reaches the reference speed in a span of 0.13 s following load application. The sudden release of the load causes increase in the speed to 1250 and settling to the reference speed again within 0.14 s. Increases in torque and stator current are also seen during the dynamic disturbance moments, as shown in Fig. 14. Uniformity of the torque is seen throughout the steady-state condition. The table 4 shows the values of odd and even harmonics of voltage and current for no-load and dynamic responses. The values of RMS voltage and current, THD and HSF for no-load and dynamic responses are shown in Table 5. The gain values of PI and ANN controllers provide the best performance in the vector control system. The THD values of stator voltage and current with load are 3.014 % and 3.971 %, respectively.

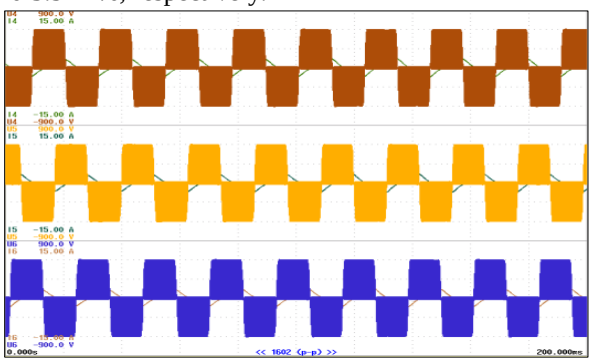

Fig. 15. Stator voltage and stator current wave forms (V_a,V_b,V_c and I_a,I_b,I_c) at the load of 1.8A.

4.3 Reference Step Response:

A start in the test was made with the IM with a set speed of 1200 rpm. This was increased to 1400 rpm. The response was settled within 0.2 s. The step response to speed, torque, and flux is shown in Fig. 16. The flux produced was constant during the speed change from 1200 to 1400 rpm and was independent of speed. It remained constant all through the wide range of speed. The torque was also uniform during the entire speed range.

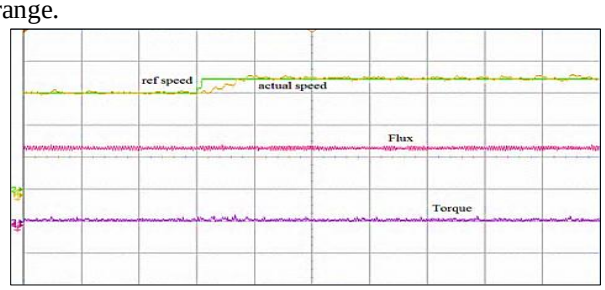

Fig. 16. Step change of speed (1200–1400) rpm, torque, and flux. (Y-axis: Speed: 2 v/div = 400 rpm; X-axis: 200 ms/div).

4.4 PWM Pulses:

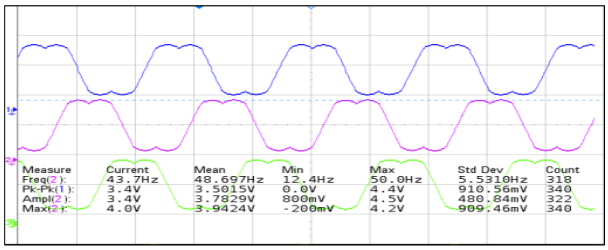

Fig. 17. Low-pass-filtered waveform of phase A, B, C drive signals of the modified SVPWM (*V:* 2 V/div; *t*: 10 ms/div).

The desired dead band time of 4 µs was hardcoded in the program itself. The phase A, B, C output drive signals of the modified SVPWM are shown in Fig. 17. The modified SVPWM method is shown with the function equivalent to the conventional SVPWM method. There is a small magnitude seen in this modified SVPWM method with fewer calculations needed in comparison with the conventional method. The processing time is smaller compared to the conventional method. The HSVPWM pulses generated from the FPGA kit are shown in Fig. 18 whose frequency is 10kz .Tables 6–8 show the hardware specifications of IM, proximity sensor, and inverter.

Table 9 shows the performance comparison with other works. Table 10 shows the comparative result analysis of SVPWM, RPWM and HSVPWM. Fig. 19 shows the hardware setup.

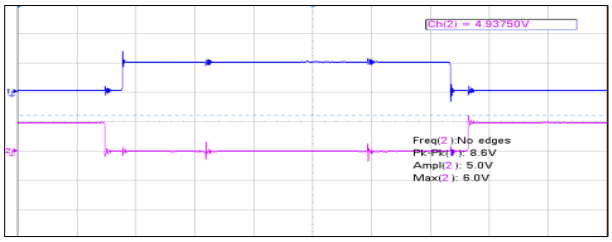

Fig. 18. Pulses fed to top and bottom IGBT's of one leg of inverter. (*V:* 5 V/div; *t*: 10 µs/div).

Table 5. Voltage, Current THD and HSF at No Load

	V_{rms}	I_{rms}	V_{THD}	I_{THD}	HSF	
					Voltage	Current
No-load response	367.86	0.8896	5.875	2.213	1.6	1.5
Dynamic response	363.59	1.8146	3.041	3.971	2.0	1.9

Table 6. Specification of a Sensor

Model	IP18305
Brown	+ive 5 to 30 V DC
Blue	-ive common
Black	Output

Table 7. Specifications of the Induction Motor Setup Used

Phase	3ph
Rated voltage	415 V (star connected)
Rated current	1.8A
Power	1.5hp
Rated speed	1415 rpm
Power factor	0.8
Stator resistance	1.405
Stator inductance	0.005839
Rotor resistance	1.395
Rotor inductance	0.005839
Mutual inductance	0.1722
Inertia	0.0131
Fraction factor	0.002985
Pole pairs	2

Table 8. Specification of IGBT-based Inverter Module

PWM INPUT		IGBT & RECTIFIER	
Amplitude	0-3.3/5V	V_{max}	750V
F_{max}	20KHz	$V_{nominal}$	650V
$F_{nominal}$	18KHz	I_{max}	25A
Dead time	6µs	$I_{nominal}$	15A
ADC range	0-3.3V	P_{max}	10KVA

Table 9. Performance Comparison

Time domain specification	Proposed work	Fu et al. [7]	Pinto et al. [8]	Muthukumar et al. [26]	Arulmozhiyaly et al. [28]	Boopathi et al. [29]
Peak overshoot	Nil	25%	-	-	26%	-
Settling time	0.6 s	1.5 s	-	-	1.6 s	-
THD	2.21 %	-	-	-	-	-
HSF	1.52	-	-	4.35 (Open loop)	-	4.48 (Open loop)
Torque	Uniform	Less Ripple	Less Ripple	-	-	-
Flux	Constant	-	Slight fluctuation	-	-	-
Usage of Resources	Flip flop -58% LUT-15% Slices-6%	-	-	-	Flip flop -14% LUT-68% Slices-88%	-

Table 10.Fundamental, HSF, THD assessment of SVPWM, RPWM, and HSVPWM

SPEED	SVPWM			RPWM			HSVPWM		
rpm	Fundamental voltage	HSF	I_{THD}	Fundamental voltage	HSF	I_{THD}	Fundamental voltage	HSF	I_{THD}
1000	354.21	4.38	5.65	309.54	4.34	7.76	359.50	2.09	2.65
1200	471.18	3.12	5.44	411.18	3.10	7.54	475.92	1.70	2.43
1400	587.71	2.07	5.12	513.68	2.15	7.32	590.31	1.50	2.21

5. Conclusion

This article has presented ANN-based vector control method for three-phase IM with HSVPWM using FPGA. The decoupling of torque and flux control was ensured by the vector control of the IM, which provided the facility of control over the IM motor linearly as a dismembered excited DC motor for the offer of an excellent dynamic response. The results tested by to the success of the HSVPWM methods vis-a-vis improved fundamental component reduced THD and minimal HSF. The strategy is considered appropriate for the modern AC drives for noise-free working. The performances such as percentage of resource usage of FPGA and THD have been enriched compared to related work [10],[21-22]. The value of HSF is lesser compare to the work done in [39], [40].The setup in this method has also found a blend with FPGA occupies a smaller area and achieves a low propagation delay with less power dissipation. More randomization can be performed using 16-bit or 32-bit linear feedback shift registers in future. This high-performance vector control system can be used in industrial applications such as process control, paper mills, steel mills, mining, and smelting plants.

(a)

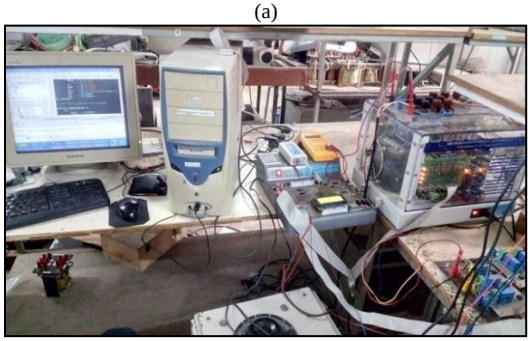

(b)

Fig. 19 (a and b) Photographs of the experimental setup.

Appendix

$L_{r,s,m}$	Rotor, stator and mutual Inductance.
$R_{r,s}$	Rotor, stator resistance.
$V_{a,b,c}$	Phase voltage
J	Rotor inertia referred to motor Shaft
θ_r	rotor electrical angle
$V^*_{d,q}$	Direct and quadrature component of stator voltage component
p	number of pole pairs
$\theta_{\lambda r}$	rotor flux position
i_{mR}	magnetizing rotor current
f_s	speed of rotor
T	sampling period
ω_b	the speed of electrical nominal
$i_d^{\lambda r}$, $i_q^{\lambda r}$	currents in the *d,q* rotating reference frame aligned with the rotor flux vector.
i_{dref}	flux reference (rotor flux command for every speed reference)
i_{qref}	torque reference (torque command)
V_d^*, V_q^*	reference voltage with respect to d,q components(output of current regulator)
V_α^* , V_β^*	the components of the stator vector voltage in the α,β orthogonal reference frame.

References

1. R. Krishnan.: (*Electric Motor Drives Modeling, Analysis, and Control*). Upper Saddle River, NJ: Prentice-Hall, 2001.
2. N. Mohan.: (*Advanced Electrical Drives: Analysis, Control And Modeling Using Simulink*). Minneapolis, MN, USA: MNPERE, 2001.
3. Kyoung-Min Kwon, Jae-Moon Lee, Jin-Mok Lee, and JaehoChoI.: (*SVM Over modulation Scheme of Three-Level Inverters for Vector Controlled Induction Motor Drives*). Journal of Power Electronics, Vol. 9, No. 3, May 2009.
4. M. Valan Rajkumar a, P.S. Manoharan b.: (*FPGA based multilevel cascaded inverters with SVPWM algorithmfor photovoltaic system*). Solar Energy 87 (2013) 229–245 SCIENCE DIRECT ELSEVIER.
5. Lim, Y.-C., Wi, S.-O., Kim, J.-N. and Jung, Y.-G.: (*A Pseudo Random Carrier Modulation Scheme*). IEEE Transactions on Power Electronics, 25, 2010, 797-805.
6. Sutikno T, Jidin A, Basar MF.: (*Simple Realization of 5-Segment Discontinuous SVM Based on FPGA*). International Journal of Computer and Electrical Engineering. 2010;2:148-57.
7. Xingang Fu and Shuhui Li.: (*A Novel Neural Network Vector Control Technique for Induction Motor Drive*). IEEE Transactions On Energy Conversion, Vol. 30, No. 4, December 2015.

8. João O. P. Pinto, Bimal K. Bose and Luiz Eduardo Borges da Silva.: (*A Stator-Flux-Oriented Vector-Controlled Induction Motor Drive With Space-Vector PWM and Flux-Vector Synthesis by Neural Networks*). IEEE Transactions On Industry Publications, Vol. 37, No. 5, September/October 2001.
9. Epaminondas D. Mitronikas and Athanasios N. Safacas.: (*An Improved Sensorless Vector-Control Method for an Induction Motor Drive*). IEEE Transactions On Industrial Electronics, Vol. 52, No. 6, December 2005.
10. Da Zhang and Hui Li.: (*A Stochastic-Based FPGA ontroller for an Induction Motor Drive With Integrated Neural Network Algorithms*). IEEE Transactions On Industrial Electronics, Vol. 55, No. 2, February 2008.
11. Yen-Shin Lai and Ye-Then Chang.: (*Design and Implementation of Vector-Controlled Induction Motor Drives Using Random Switching Technique with Constant Sampling Frequency*). IEEE Transactions On Power Electronics, Vol. 16, No. 3, May 2001.
12. Haibing Hu, Wenxi Yao and Zhengyu Lu.: (*Design and Implementation of Three-Level Space Vector PWM IP Core for FPGAs*). IEEE Transactions On Power Electronics, Vol. 22, No. 6, November 2007.
13. Lazhar Ben-Brahim Ryoichi Kurosawa.: (*Identification of Induction Motor Speed using Neural Networks*). THMOG-9/93 IEEE, 1993.
14. Kim, K.-S., Jung, Y.-G. and Lim, Y.-C.: (A New Hybrid Random PWM Scheme. IEEE Transactions on Power Electronics, 24, 192-200, 2009.
15. Thomas G. Habetler and Deepakraj M. Divan.: (*Acoustic Noise Reduction in Sinusoidal PWM Drives Using a Randomly Modulated Carrier*). IEEE Transactions on Power Electronics, vol. 6, NO. 3, July 1991
16. D. W Novotny and T.A. Lipo.: (*Vector Control and Dynamics of AC Drives*). Oxford Science Publications, ISBN 0-19-856439-2.
17. B.Hariram, Dr.N.S.Marimuthu.: (*Evaluation of FPGA based speed control of Induction Motor*). Journal of Electrical Engineering.
18. Azuwien Aida Boharia, WahyuMulyoUtomoa, ZainalAlamHarona, NooradzianieMuhd.Zina, Sy Yi Sim, and Roslina Mat Ariff.: (*Speed Tracking of Indirect Field Oriented Control Induction Motor using Neural Network*). Procedia Technology 11 (2013) 141 – 146 Science direct Elsevier.
19. J. Dannehl, C.Wessels and F.W. Fuchs.: (*Limitations of voltage-oriented pi current control of grid-connected PWM rectifiers with LCL filters*). IEEE Trans. Ind. Electron., vol. 56, no. 2, pp. 380–388, Feb. 2009.
20. Arzhang Yousefi-Talouki, Gianmario Pellegrino.: (*Sensorless Control of Matrix Converter-Fed Synchronous Reluctance Motors Based on Direct Flux Vector Control Method*). Journal of Electrical Engineering, vol 17, 2nd edition, 2017.
21. S. Haykin.: (*Neural Networks*). AComprehensive Foundation. Macmillan College Publislhing Company, 1994.
22. Michael T. Wishart and Ronald G. Harley.: (*Identification and Control of Induction Machines Using: Artificial Neural Networks*). IEEE Transactions On Industry Applications, Vol. 31, No. 3, May/June 1995.
23. Donald Grahame Holmes, Brendan Peter McGrath and Stewart Geoffrey Parker.: (*Current Regulation Strategies for Vector-Controlled Induction Motor Drives*). IEEE Transactions On Industrial Electronics, Vol. 59, No. 10, October 2012.
24. J. S. Lai and F. Z. Peng.: (*Multilevel converters–A new breed of power converters*). IEEE Trans. Ind. Applicat., vol. 32, pp. 509–517,May/June 1996.
25. Ahmad Radan and Zahra Daneshi Far.: (*Optimization Opportunities in carrier-based Multilevel PWM using Degrees of freedom of modulation*".
26. Muthukumar Paramasivan, Melba Mary Paulraj, Sankaragomathi Balasubramanian.: (*Assorted carrier-variable frequency-random PWM scheme for voltage source inverter*). IET Power Electron.© The Institution of Engineering and Technology 2017, ISSN 1755-4535.
27. Krishnakumar, C., Muhilan, P., Sathiskumar, M. and Sakthivel, M.: (*A New Random PWM Technique for Conducted- EMI Mitigation on Cuk Converter*). Journal of Electrical Engineering & Technology, 10, 916-924, 2015.
28. R.Arulmozhiyaly and K. Baskaran.: *(Implementation of a Fuzzy PI Controller for Speed Control of Induction Motors Using FPGA*). Journal of Power Electronics, Vol. 10, No. 1, January 2010.
29. R.Boopathi, P.Muthukumar, P.Melba Mari, S.Jeevananthan.: (*Investigations on Harmonic Spreading Effects of SVPWM Switching Patterns in VSI fed AC Drives*). IEEE - International Conference On Advances In Engineering, Science And Management (ICAESM -2012) March 30, 31, 2012.

Rajan.V.R received the B.E. degree in Electrical and Electronics engineering in 1998 Manonmanium Sundaranar University, Tirunelveli and the M.E. degree in power electronics and drives in 2006 from Govt. College of Technology, Coimbatore, and Anna University, India. He is currently an assistant professor at Electrical and Electronics Engineering Department of V V College of Engineering, Thisaiyanvilai, and Tirunelveli, India.

Dr.K. Selvi obtained B.E EEE with Honours, M.E Power System with Distin, from Madurai Kamaraj University in the year 1989 and 1995 respectively. She obtained Ph.D in Electricity Deregulation in June 2005 from Madurai Kamaraj University. She is currently working as Assistant Professor in Department of Electrical Engineering, in Thiagarajar college of Engineering, Madurai, Tamilnadu, India. She has obtained Young Scientist Fellowship from Dept. of Science and Technology. Her research interests are Electricity deregulation and AI techniques.